

## Raman scattering study of coalesced single walled carbon nanotubes

S. L. Fang, A. M. Rao, and P. C. Eklund<sup>a)</sup>

*Department of Physics and Astronomy and Center for Applied Energy Research, University of Kentucky, Lexington, Kentucky 40506*

P. Nikolaev, A. G. Rinzler, and R. E. Smalley

*Center for Nanoscale Science and Technology, Rice Quantum Institute, and Departments of Chemistry and Physics, Rice University, Houston, Texas 77251*

(Received 6 April 1998; accepted 1 June 1998)

High temperature heat treatment of single wall carbon nanotube bundles in flowing H<sub>2</sub> was used to produce a significant fraction (~40%) of diameter-doubled, or coalesced tubes with a mean diameter corresponding to that of ~(20, 20) tubes. At three laser excitation wavelengths (514.5, 647, and 1064 nm), a reduction in the Raman scattering intensity of the strong radial and tangential modes was observed in the H<sub>2</sub>-treated sample, consistent with the reduced fraction of tubes in the sample after coalescence. However, using 488 nm excitation, little or no change is observed in the Raman spectrum after the H<sub>2</sub> treatment, suggesting that this excitation wavelength couples only to chiral symmetry tubes. Using the 647 nm excitation, the effect of H<sub>2</sub> treatment on the tangential band is quite unique, and a significant change in the shape of the tangential band was observed. Our lineshape analysis, and other results reported in this issue, suggest that this unique change of shape is due to lost scattering intensity from metallic tubes partially compensated by tangential mode scattering from the coalesced tubes. The normally prominent radial breathing mode band, which would be expected at ~90 cm<sup>-1</sup> for ~(20, 20) tubes was not observed, indicating that these larger diameter tubes do not exhibit strong resonant scattering, at least at any of the wavelengths used in this study.

### I. INTRODUCTION

Synthesis of single-walled carbon nanotubes (SWNT's) in bulk quantities has become possible after the discovery of the pulsed laser vaporization (PLV)<sup>1</sup> and the electric arc growth methods<sup>2</sup> at Rice and Montpellier Universities, respectively. Some of the physical properties of these one-dimensional (1D) materials have been determined from studies on the PLV-derived SWNT material.<sup>1,3-11</sup> The large aspect ratio (length-to-diameter  $\geq 10^3$ ) of the SWNT's confines the electron motion to the nanotube axis, and depending on the tube diameter and chirality, either metallic or semiconducting tubes are obtained.<sup>3</sup> Single-molecule transistor behavior has been demonstrated by Tans *et al.*<sup>5</sup> and Bockrath *et al.*<sup>4</sup> in carbon nanotube-based devices that were fabricated using photolithographic techniques. Raman scattering from small diameter SWNT's has also provided important information about the diameter-dependent electronic and vibrational properties.<sup>6,12</sup> A resonant Raman scattering process was observed, and this resonance was assigned to the 1D quantum confinement of the electrons in the nanotube.<sup>6,13</sup>

Nikolaev *et al.*<sup>14</sup> have reported that SWNT bundles rich (as much as 60 vol %) in ~(20, 20) tubes can be obtained by annealing the as-prepared ~(10, 10) bundles at 1500 °C in a flowing hydrogen atmosphere. Analysis of TEM contrast images of annealed bundles also indicated the presence of few ~(30, 30) tubes (~2 vol %).<sup>14</sup> This experimental observation of diameter doubled (and tripled) SWNT's in the annealed bundles was interpreted in terms of a "coalescence" between neighboring ~(10, 10) SWNT's within the bundle.<sup>14</sup> It was further suggested that (i) the coalescence of smaller diameter tubes is thermodynamically favored since the resulting larger diameter tubes effectively reduce the strain energy; and (ii) since only nanotubes with equal helical pitch and chirality can coalesce seamlessly without major atomic C-atom rearrangement within the wall, the high conversion rate to ~(20, 20) SWNT's corroborates earlier conclusions from electron nanodiffraction work that the PLV growth technique, to a large extent, favors strongly the growth of metallic armchair tubes.<sup>15</sup> However, it must be noted that atomically resolved scanning tunneling microscopy (STM) images of isolated SWNT's and bundles have found an apparent contradiction of the view that the (10, 10) tubes are predominantly present in PLV-derived samples.<sup>10,11</sup> Similar conclusions were

<sup>a)</sup>Address correspondence to this author.

made from an earlier Raman scattering study on PLV-derived SWNT bundles.<sup>6,12</sup>

In the present study, we investigate the changes in the Raman spectrum of SWNT bundles, before and after coalescence, to further elucidate the diameter-dependence of the vibrational mode frequencies and intensities. In interpreting our results, we are making a tacit assumption that the adjacent chiral tubes cannot coalesce under the present experimental conditions. This view has been argued at length in a previous publication.<sup>14</sup>

## II. EXPERIMENTAL DETAILS

The SWNT's used in this study were produced in a PLV apparatus similar to one described previously.<sup>1</sup> A composite graphite target containing 1:1 at. % of Co:Ni catalyst was maintained at 1200 °C inside a flow tube furnace. Ablation pulses were provided by two Q-switched Nd:YAG lasers which delivered 480 mJ/pulse and 560 mJ/pulse of 532 nm (9 ns, 30 Hz, 6.4 mm diameter spot) and 1064 nm radiation, respectively. The latter was co-axial and delayed by 42 ns with respect to the former pulse.<sup>1</sup> Electron microscopy studies of the resulting carbon material revealed that bundles of aligned SWNT's were present as the majority fraction (yield 70% to 90%), together with other *sp*<sup>2</sup>-bonded carbon nanospheres, metal nanoparticles, and fullerenes.<sup>1,16</sup>

Measurements of SWNT diameters were made from transmission electron microscope (TEM) images obtained with a JEOL 2010 TEM. Imaging was restricted to cases in which a rope curved through the focal plane of the microscope affording essentially a "cross-sectional" view of the tubes comprising the rope. To enhance the number of such cases, the sample to be imaged was prepared by tearing out a strand of the SWNT material from the felt, laying it on a holey carbon TEM grid supported on blotting paper, and wetting with a drop of methanol to adhere the strand to the grid. This approach differs from the more standard technique of dispersing the sample by sonication in methanol and placing a drop of the material on the grid. The accuracy in the measured tube diameters is estimated to be  $\pm 0.15$  nm. In the high resolution TEM images, it was observed that typical bundles consisted of 100–500 SWNT's held together by weak van der Waals bonding to form a 2D triangular lattice with a lattice constant of 17 Å.<sup>1</sup> From such TEM images, a very narrow diameter distribution (1.0 to 1.6 nm) centered near 1.3 nm was obtained. In the standard notation,<sup>3</sup> this mean value corresponds approximately to that of  $\sim(10, 10)$  nanotube.

For the samples used in this study, the SWNT bundles rich in  $\sim(20, 20)$  tubes were prepared in the same way as described in Ref. 14. About 10 mg of as-prepared SWNT felt was placed in an alumina boat

within an alumina flow tube furnace. The flow tube was evacuated with a turbo-pump and the furnace temperature was ramped to 1000 °C. After 5.5 h the pressure stabilized at  $4 \times 10^{-5}$  Torr, at which time the turbo-pump was throttled back and 99.999% hydrogen was introduced at a flow rate of 2 sccm. The furnace was then ramped at 10 °C/min to 1500 °C at which temperature the material was held in the flowing hydrogen background at a pressure of  $2.6 \times 10^{-3}$  Torr for 4 h.

Raman scattering measurements were carried out with (i) 488 nm, 514.5 nm (Ar ion laser), and 647 nm (Kr ion laser) excitations and a Jobin Yvon HR460 single grating spectrometer equipped with a liquid-nitrogen-cooled, charge-coupled array detector and a holographic notch filter (Kaiser Optical); and (ii) with 1064 nm excitation (Nd:YAG) in a Fourier transform interferometric spectrometer (Bomem DA3<sup>+</sup>) equipped with a liquid-nitrogen-cooled GaInAs detector. The spectral slitwidths for the Jobin Yvon HR460 and the Bomem DA3<sup>+</sup> were  $\sim 2$  cm<sup>-1</sup> and  $\sim 4$  cm<sup>-1</sup>, respectively. Raman data for the SWNT bundles before, and after the H<sub>2</sub> treatment were collected under identical experimental conditions (i.e., same laser power and alignment conditions). This was accomplished by translating first the pristine, and then the H<sub>2</sub>-treated sample, into the laser beam and successively collecting the respective Raman spectra. In effect, successive Raman spectra were therefore collected by exact substitution of the two samples to be compared.

## III. RESULTS AND DISCUSSION

Figures 1(a) and 1(b) show, respectively, a representative cross-sectional view of the bundles before and after the coalescence reaction. Clearly, the triangular packing of the SWNT's which forms the rope lattice can be observed in the figure; the tube diameter distribution in our sample was determined from these images, such as shown in Figs. 1(a) and 1(b). In Fig. 1(b), the diameter doubled SWNT's appear somewhat "oval" in cross-sectional view as they bend through the focal plane of the microscope, and hence average diameters were determined for these wider nanotubes. Occasionally, as indicated by the arrow in Fig. 1(b), adjacent wider tubes exhibit deformations which increase their contact areas. Typical diameter histograms determined from images, such as shown in Fig. 1 on the same material, before and after the coalescence reaction, are shown in Figs. 2(a) and 2(b). The total number of tubes sampled in Figs. 2(a) and 2(b) are obviously different, since the same area of the sample cannot be imaged before and after the high temperature treatment in hydrogen. Neglecting the small fraction of diameter-tripled and diameter-quadrupled tubes in the analysis, the fraction (*f*) of tubes that have coalesced into double-diameter

tubes can be estimated from Fig. 2(b) using

$$f = 2N_{2d}/(N_d + 2N_{2d}), \quad (1)$$

where  $N_d$  and  $N_{2d}$  refer, respectively, to the number of tubes with diameter  $d$  and  $2d$ . From a total of 160 diameter measurements, the fraction  $f$  of the tubes that are diameter-doubled tubes is estimated using Eq. (1) to be  $\sim 42\%$ . This is somewhat less than reported previously under similar conditions ( $\sim 60\%$ <sup>14</sup>).

The distinctive features in the Raman spectra for SWNT bundles prepared by arc and PLV methods include two strong first-order bands at  $\sim 180 \text{ cm}^{-1}$  and  $\sim 1590 \text{ cm}^{-1}$ .<sup>2,6</sup> The former band has been identified with the  $A_{1g}$  symmetry radial breathing modes (RBM) which exhibit a strong dependence of mode frequency on nanotube diameter. The latter band has been assigned on an unresolved Raman triplet ( $A_{1g}$ ,  $E_{1g}$ , and  $E_{2g}$ ) identified with tangential carbon displacement modes.<sup>6</sup> These three, nearly degenerate, nanotube phonons are related to the graphite  $E_{2g}$  symmetry intralayer mode at  $1582 \text{ cm}^{-1}$  and exhibit a relatively weak dependence of frequency on tube diameter. Besides the strong Raman-active radial and tangential modes in the as-prepared SWNT bundle,  $\sim 8$  weak peaks have also been observed for PLV-derived material in the range  $300\text{--}1400 \text{ cm}^{-1}$ .<sup>6</sup>

Because the SWNT vibrational mode frequencies depend on diameter,<sup>6</sup> the Raman peaks of SWNT's are inhomogeneously broadened due to the inherent tube diameter distribution present in the material.<sup>6,12</sup> All the first-order, low frequency ( $\omega < 400 \text{ cm}^{-1}$ ) modes have been shown theoretically<sup>13,17</sup> to exhibit a strong frequency dependence on diameter. In particular, the frequency of the  $A_{1g}$  symmetry RBM, in which all of the carbon atoms undergo an equal radial displacement, is strongly diameter-dependent, and therefore the radial mode frequency can, in principle, be used to measure the tube diameter.<sup>6,12</sup> An empirical expression for the RBM frequency ( $\omega_r$ ) is given by the formula

$$\omega_r(d) = 223.75 (\text{cm}^{-1} - \text{nm})/d, \quad (2)$$

where  $\omega_r$  is measured in wave numbers, and  $d$  is measured in nanometers. This result is found to be independent of chirality; i.e., it applies to all tube types (armchair, zigzag and chiral).<sup>13,17</sup> This inverse relation between  $\omega_r$  and  $d$  was obtained by two research groups using an empirical force constant model employing the C–C force constants that were used to fit the two-dimensional, experimental phonon dispersion of a single graphene sheet.<sup>13,17</sup> The results of Saito *et al.*<sup>17</sup> were fit to the function  $\omega_r(d) = ad^{-n}$ , and they find  $a = 224.02 (\text{cm}^{-1} - \text{nm})$  and  $n = 1.0017$ ; whereas our approach was to carry out a least squares fit of the calculated frequencies to the function  $a/d$  (i.e.,  $n = 1$ ).

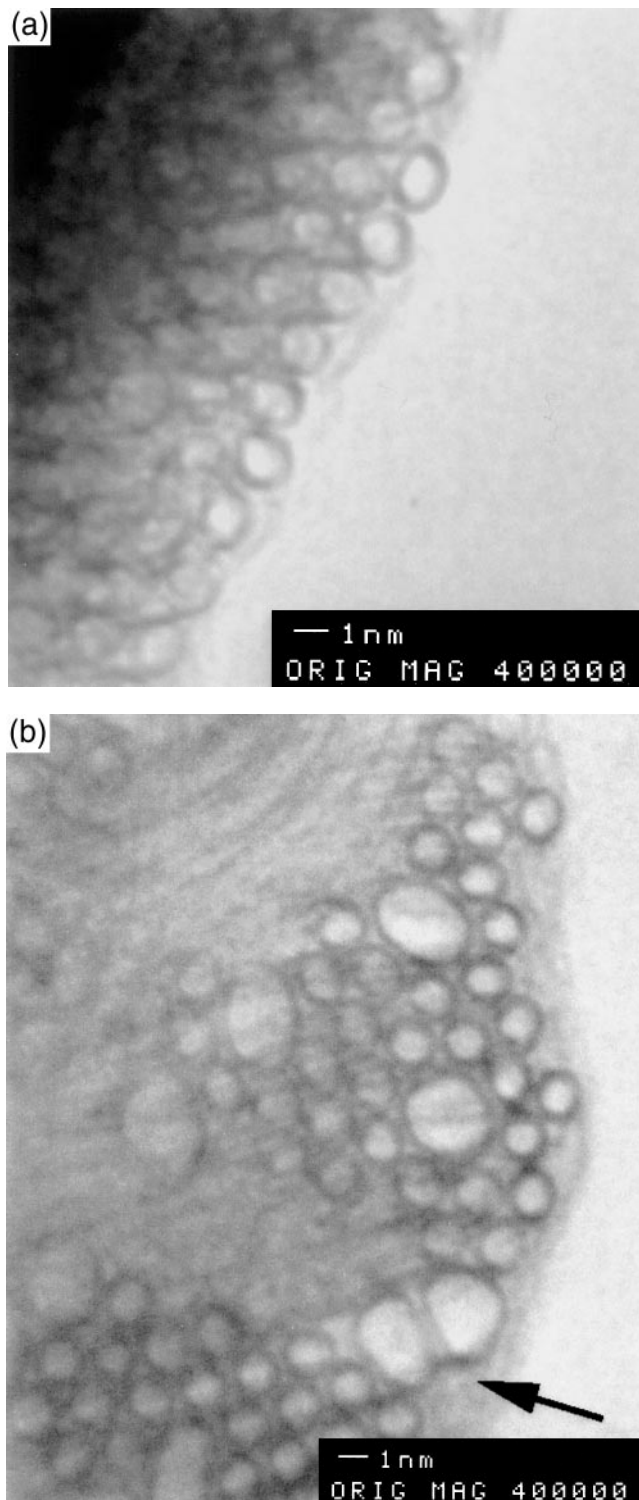


FIG. 1. TEM cross-sectional view of the bundles before (a) and after (b) the coalescence reaction (see text). Adjacent wider tubes exhibit deformations which increase their contact areas [indicated by the arrow in Fig. 1(b)].

In Figs. 3(a) and 3(b), respectively, we show Raman bands from the low and high frequency regions containing resonant scattering from the radial and tangential

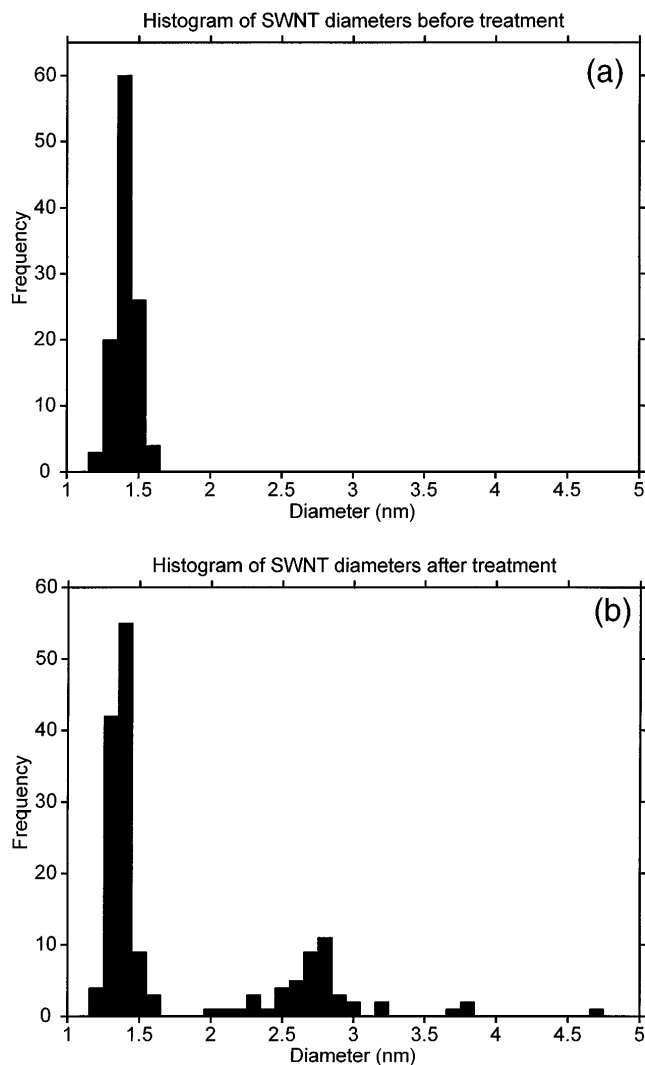


FIG. 2. Typical diameter histograms determined from TEM cross-sectional images (such as shown in Fig. 1), before (a) and after (b) the coalescence reaction.

modes. Data for the pristine and  $H_2$ -treated tubes are shown, respectively, as the dashed and solid traces. When appropriate, we also plot for comparison a scaled version of the pristine spectrum; i.e., a new spectrum is created by multiplying the pristine spectrum by a wave number-independent, constant scale factor ( $\alpha$ ). Values for  $\alpha$  and the laser excitation wavelength appear to the left and right of each spectrum, respectively. Four excitation wavelengths have been used to study the effect of the coalescence. Each of these wavelengths is expected to excite resonant scattering from four different populations of tubes within the sample (i.e., different diameter and symmetry tubes).<sup>6</sup> The average value we find for  $\alpha$  via analysis of the Raman data, i.e.,  $\alpha_{\text{avg}} = (0 + 0.588 + 0.556 + 0.714)/4 = 0.46$ , is in reasonable agreement with the TEM-derived value ( $\alpha \sim 0.42$ ) for the fraction of pristine tubes that have coalesced.

We consider first the results for the radial modes [Fig. 3(a)]. For the case of 514.5 nm and 647 nm excitation, it can be seen that the radial band of the  $H_2$ -treated sample is well fit by that of a Raman spectrum which is simply a scaled replica of the Raman spectrum of the pristine material. This successful scaling indicates that all the tube symmetries in the population sampled with the particular wavelength has suffered a uniform reduction in their number as a result of the coalescence reaction. That is, because  $\sim(10, 10)$  tubes coalesce to become  $\sim(20, 20)$  tubes, their scattering intensity is lost from the radial band in the figure, and is anticipated to appear at a much lower frequency because of the inverse diameter dependence of the RBM frequency [Eq. (2)]. However, no new feature near  $\sim 90 \text{ cm}^{-1}$  was observed in the Raman spectrum of coalesced SWNT's for all four excitation wavelengths. This observation is consistent with calculated intensities for the resonantly enhanced SWNT modes, which indicate that for a fixed excitation frequency, the calculated Raman cross section decreases strongly with increasing tube diameter.<sup>13</sup> Furthermore, it was also noted in Ref. 13 that, in the limit of infinite diameter (graphene sheet), the Raman cross section for this resonance should vanish. Our data indicate that the Raman cross section for the radial breathing mode of a  $\sim(20, 20)$  tube with diameter  $d \sim 2.7 \text{ nm}$  is too weak to observe with visible and Nd:YAG (1064 nm) laser excitations.

For the case of 1064 nm excitation, scaling the pristine spectrum produces a reasonable fit to the high, but not the low, frequency component in the radial doublet, indicating that the larger diameter tubes in this population were selectively destroyed or coalesced. Interestingly, using 488 nm excitation, the shape of the radial band and its Raman scattering intensity obtained remains unchanged upon  $H_2$  treatment. This indicates that the population of tubes excited to resonantly scatter with 488 nm radiation is unaffected by the  $H_2$  treatment and the coalescence of certain nanotubes. As discussed in the introductory remarks, adjacent chiral tubes are not expected to coalesce because they cannot exhibit a commensurate seam along their length, contrary to the situation with adjacent armchair or zigzag tubes. Therefore, the independence of the 488 nm Raman data to  $H_2$  treatment, taken together with the fact that  $\sim 40\%$  of the  $\sim(10, 10)$  tubes are lost from the initial population due to coalescence, suggests that the population of pristine tubes sensitive to 488 nm excitation can be characterized as primarily chiral. Thus, 488 nm may be a good excitation wavelength to probe the chiral tube population within a sample.

We next consider the effect of the  $H_2$  treatment and resulting coalescence on the high frequency tangential band with its largest component centered at  $\sim 1590 \text{ cm}^{-1}$ . The results for the four laser excitation

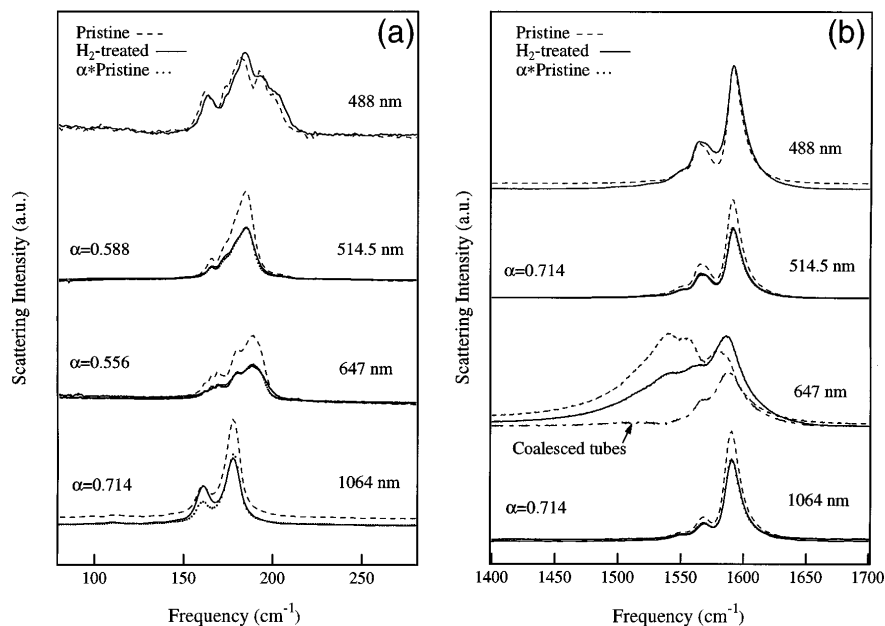


FIG. 3. Resonant Raman scattering bands from the radial (a) and tangential (b) SWNT modes. Data for the pristine and H<sub>2</sub>-treated tubes are shown, respectively, as the dashed and solid traces. The dotted traces were obtained by multiplying the pristine spectrum by a wave number-independent, constant scale factor  $\alpha$ . The dash-dotted trace is computed as  $I_{-(20,20)} = I_{\text{H}_2 \text{ treated}} - 0.556I_{\text{Pristine}}$  and is assigned to Raman scattering intensity from coalesced tubes (see text).

wavelengths are shown in Fig. 3(b), and the dashed, solid, and dotted lines have the same meaning as described above for Fig. 3(a). For 514.5 nm and 1064 nm excitations, it can be seen that the same, or nearly the same, values for  $\alpha$  that were used to interpret the reduction in intensity of the radial band upon H<sub>2</sub> treatment [Fig. 3(a)] can be also used to explain the reduced intensity of the tangential band after H<sub>2</sub> treatment. In fact, we expect  $\alpha$  to be slightly higher for the tangential band analysis than for the radial band. In this case, the larger diameter coalesced tubes can also make a contribution to the 1590 cm<sup>-1</sup> band since the diameter-dependence of the tangential mode frequency is relatively weak. This is not the case for the radial band, as the coalesced tubes exhibit a much lower radial band frequency due to the diameter doubling, and the contribution from the diameter-doubled tubes shifts out of the band assigned to the pristine material. In other words, some of the tangential mode scattering intensity lost by the coalescence of the smaller, pristine tubes is compensated by the tangential mode scattering from the  $\sim(20,20)$  tubes. The scattering from the  $\sim(20,20)$  tubes is probably not strongly resonant because of the much larger tube diameter; i.e., for such a large diameter ( $d \sim 27 \text{ \AA}$ ) the system is attaining the scattering characteristics of a planar graphene sheet,<sup>13</sup> which is not expected to exhibit resonant Raman scattering at these excitation frequencies. We note that  $\alpha$  is about the same for the tangential and radial bands for 1064 nm excitation, consistent with the view that this excitation

energy is very far from resonance in a  $\sim(20,20)$  tube. For 488 nm excitation of the tangential mode scattering, similar to that found for the radial band, no change in intensity is observed upon H<sub>2</sub> treatment. Consistent with the interpretation given above for the effect of H<sub>2</sub> treatment or coalescence on the radial band, we interpret the observed *independence* of the tangential band to H<sub>2</sub> treatment as further experimental evidence that 488 nm excitation favors scattering from chiral tubes.

Using 647 nm excitation, the effect of the H<sub>2</sub> treatment on the tangential band is unique compared to the other three excitation wavelengths and is discussed separately [see Fig. 3(b)]. As observed previously,<sup>6</sup> and also discussed in another paper in this issue,<sup>18</sup> Raman excitation of pristine nanotubes in the red ( $\sim 2 \text{ eV}$ ) produces a broadened and downshifted tangential band [Fig. 3(b)], altogether different in shape from the tangential bands observed with other excitation wavelengths. This difference has been attributed recently<sup>18</sup> to scattering from *metallic* tubes. Briefly, this assignment is based on results from electronic density of states (DOS) calculations<sup>19</sup> for a variety of carbon nanotubes within the tube diameter range found for the pristine sample. The calculated DOS show that *metallic* chiral, zigzag, and armchair tubes exhibit a  $\sim 2 \text{ eV}$  energy separation between mirror image  $E^{-1/2}$  singularities in the valence and conduction bands, and therefore these metallic tubes should exhibit an enhanced Raman cross section for  $\sim 2 \text{ eV}$  incident photons (647 nm = 1.92 eV). Consistent with this view is the experimental observation of a

broadening and downshifting of the Raman lines in the tangential band, which is consistent with a metallic system exhibiting an enhanced electron-phonon contribution to the Raman-active phonon linewidth. As shown on an expanded frequency scale in Fig. 4, the 647 nm-excited tangential band is clearly downshifted and broadened. Our Lorentzian lineshape analysis shows that the broadened tangential band (upper spectrum) is reasonably fit using a rigid downshift of all components in the band ( $\Delta\omega = 18 \text{ cm}^{-1}$ ) and with an enhanced broadening of the full-width at half-maximum intensity (FWHM)  $\Delta\Gamma = 30 \text{ cm}^{-1}$  relative to the linewidth obtained with the 514.5 nm excitation (lower spectrum in Fig. 4). The upper and lower spectrum in Fig. 4 is therefore identified, respectively, with metallic and semi-conducting nanotube ropes.<sup>18</sup> After  $\text{H}_2$  treatment, this tangential band shape changes [Fig. 3(b)], and we attempt to explain this change by the dash-dotted spectrum plotted under the 647 nm data. The dash-dotted spectrum is assigned to coalesced tubes and computed as

$$I_{\sim(20,20)} = I_{\text{H}_2 \text{ treated}} - 0.556I_{\text{Pristine}}, \quad (3)$$

where  $I$  represents the Raman scattering intensity and the coefficient 0.556 is obtained from the analysis of the reduction in the intensity of the radial band after the  $\text{H}_2$  treatment [Fig. 3(a)]. Equation (3) is written to reflect our assumption throughout this paper, that the spectrum of the  $\text{H}_2$ -treated nanotube sample is the sum of two primary contributions: (i) reduced contribution from pristine tubes whose numbers have been reduced by  $\text{H}_2$  treatment, and (ii) the contribution from  $\sim(20,20)$ , or coalesced tubes. We note from Fig. 3(b) (dash-dotted spectrum; 647 nm excitation) that the  $I_{\sim(20,20)}$  tangential band calculated in this way resembles that of the typical tangential band obtained with excitations sufficiently removed from 2 eV.

#### IV. CONCLUSIONS

Comparison of the Raman spectrum before and after  $\sim 40\%$  coalescence of pristine tubes to produce diameter-doubled tubes reveals interesting excitation wavelength dependent results. Consistent with the view that coalescence favors adjacent armchair and zigzag tubes (and not chiral tubes), the present study shows that 488 nm excitation favors scattering from chiral tubes, whereas 514.5, 647, and 1064 nm primarily excite scattering from armchair and zigzag tubes. We were unable to observe the scattering from the radial band of  $\sim(20,20)$  tubes expected at  $90 \text{ cm}^{-1}$ . This may indicate that the doubled  $\sim(20,20)$  tubes are approaching the behavior of a graphene sheet with regard to resonant Raman scattering.

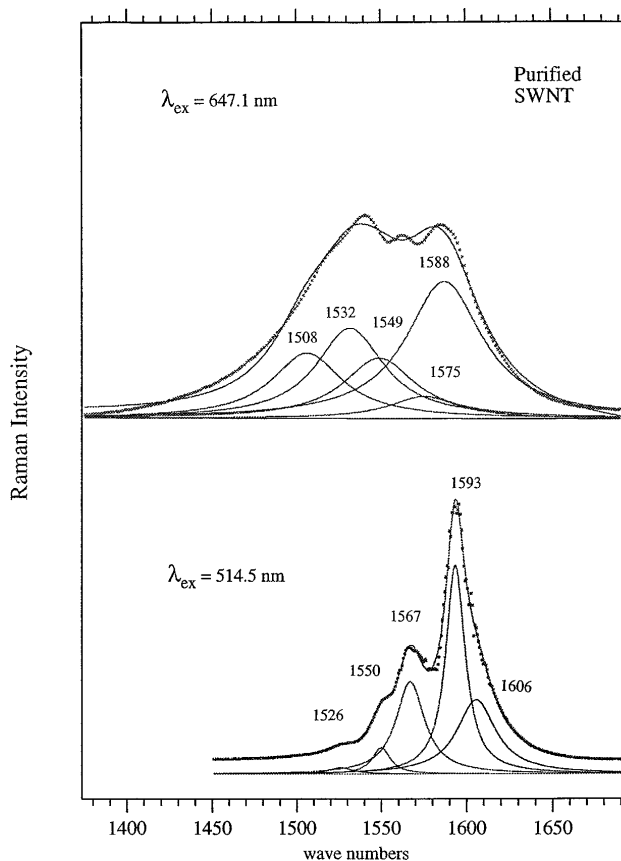


FIG. 4. Dotted spectra represent the tangential bands for the pristine SWNT sample obtained using 647 (upper spectrum) and 514.5 (lower spectrum) nm excitations. The Lorentzian lineshape analysis shows that the broadened tangential band (upper spectrum) is reasonably fit using a rigid downshift ( $\Delta\omega = 18 \text{ cm}^{-1}$ ) of all components in the band and with an enhanced broadening ( $\Delta\Gamma = 30 \text{ cm}^{-1}$ ) of the full-width at half-maximum intensity (FWHM) relative to the linewidth obtained with the 514.5 nm excitation.

#### ACKNOWLEDGMENTS

Research at the University of Kentucky (UKY) was supported by NSF Grant EPS-9452895 and the Center for Applied Energy Research at UKY. The authors thank Professor M. S. Dresselhaus, Dr. G. Dresselhaus, and Dr. M. Pimenta (M.I.T.) for helpful discussions.

#### REFERENCES

1. A. Thess, R. Lee, P. Nikolaev, H. Dai, P. Petit, J. Robert, C. Xu, Y. H. Lee, S. G. Kim, A. G. Rinzler, D. T. Colbert, G. Scuseria, D. Tomanek, J. E. Fischer, and R. E. Smalley, *Science* **273**, 483 (1996).
2. C. Journet, W. K. Maser, P. Bernier, A. Loiseau, M. Lamy de la Chapelle, S. Lefrant, P. Deniard, R. Lee, and J. E. Fischer, *Nature (London)* **388**, 756 (1997).
3. M. S. Dresselhaus, G. Dresselhaus, and P. C. Eklund, *Science of Fullerenes and Carbon Nanotubes* (Academic Press, New York, 1996).
4. M. Bockrath, D. H. Cobden, P. L. McEuen, N. Chopra, A. Zettl, A. Thess, and R. E. Smalley, *Science* **275**, 1922 (1997).

5. S. Tans, M.H. Devoret, H. Dai, A. Thess, R.E. Smalley, L.J. Geerligs, and C. Dekker, *Nature (London)* **386**, 474 (1997).
6. A.M. Rao, E. Richter, S. Bandow, B. Chase, P.C. Eklund, K.A. Williams, S. Fang, K.R. Subbaswamy, M. Menon, A. Thess, R.E. Smalley, G. Dresselhaus, and M.S. Dresselhaus, *Science* **257**, 187 (1997).
7. A.M. Rao, P.C. Eklund, S. Bandow, A. Thess, and R.E. Smalley, *Nature (London)* **388**, 257 (1997).
8. R. Lee, H.J. Kim, J.E. Fischer, A. Thess, and R.E. Smalley, *Nature (London)* **388**, 255 (1997).
9. P. Collins, A. Zettl, H. Bando, A. Thess, and R.E. Smalley, *Science* **278**, 100 (1997).
10. T.W. Odom, J. Huang, P. Kim, and C.M. Lieber, *Nature (London)* **391**, 62 (1998).
11. J.W. Wildoer, L.C. Venema, A.G. Rinzler, R.E. Smalley, and C. Dekker, *Nature (London)* **391**, 59 (1998).
12. S. Bandow, S. Asaka, Y. Saito, A.M. Rao, L. Grigorian, E. Richter, and P.C. Eklund, *Phys. Rev. Lett.* **80**, 3779 (1998).
13. E. Richter and K.R. Subbaswamy, *Phys. Rev. Lett.* **79**, 2738 (1997).
14. P. Nikolaev, A. Thess, A.G. Rinzler, D. Colbert, and R.E. Smalley, *Chem. Phys. Lett.* **266**, 422 (1997). The notation  $\sim(20,20)$  implies that the dominant tube diameter in the coalesced sample corresponds to that of the (20,20) armchair tubes ( $d \sim 27.1$  Å). Tubes with other diameters, such as (19,19), (19,20), (21,21), ..., are also present in the coalesced sample.
15. J.M. Cowley, P. Nikolaev, A. Thess, and R.E. Smalley, *Chem. Phys. Lett.* **265**, 379 (1997).
16. S. Bandow, A.M. Rao, K.A. Williams, A. Thess, R.E. Smalley, and P.C. Eklund, *J. Phys. Chem. B* **101**, 8839 (1997).
17. R. Saito, M.S. Dresselhaus, and G. Dresselhaus, *Physics of Carbon Nanotubes* (Imperial College Press, London, 1998), Chap. 4.
18. M. Pimenta, A. Marucci, S.D.M. Brown, M.J. Matthews, A.M. Rao, P.C. Eklund, R.E. Smalley, G. Dresselhaus, and M.S. Dresselhaus, *J. Mater. Res.* **13**, 2396 (1998).
19. J.C. Charlier, private communication (1998).